NJC

ROYAL SOCIETY OF CHEMISTRY

PAPER

View Article Online
View Journal | View Issue

Cite this: *New J. Chem.*, 2023, **47**, 13367

Use of a bioresource nanocomposite as a heterogeneous base catalyst for the green synthesis of novel bioactive pyrazoles: antibacterial evaluation using molecular docking†

Sarah Aldulaijan,[ab] Sara Nabil,[ab] Salha Alharthi,[ab] Bushra AL Abdullatif[ab] and Abir S. Abdel-Naby *[ab]

Received 9th November 2022,
Accepted 5th June 2023

DOI: 10.1039/d2nj05513a

rsc.li/njc

Chitosan modified with diallylamine (CS-DAA) was synthesized and mixed with nano magnesium oxide (in various percentages) to prepare CS-DAA–MgO nanocomposites for use as a heterogeneous base catalyst for the synthesis of novel pyrazole derivatives. ^{13}C NMR spectroscopic analysis confirmed the synthesis of the new functionalized chitosan CS-DAA. The nanocomposite containing 5% MgO exhibited the highest thermal stability as shown in the thermogravimetry curves. The X-ray diffraction pattern and scanning electron microscopy confirmed the formation of the nanocomposite CS-DAA–MgO. The eco-friendly, biodegradable nanocomposite was used as a heterogeneous base catalyst for the synthesis of four novel pyrazole derivatives. Pyrazolone was condensed with thiocarbohydrazide in two different ratios to afford the corresponding hydrazones (**1** and **2**). These hydrazones were treated with α-haloesters or hydrazonoyl halides in the presence of the heterogeneous nanocomposite catalyst, resulting in the formation of thiadiazines (3) and thiazolidin-4-one (4). The catalytic effect of the nanocomposite showed higher catalytic efficiency compared to the traditional homogeneous base catalysts Et_3N and NaOH. The four pyrazole structures were confirmed using elemental analysis, ^{1}H NMR and ^{13}C NMR. A molecular docking study was used to predict the inhibition potential for the four pyrazole derivatives as anti-bacterial drugs for *Escherichia coli, Pseudomonas aeruginosa, Staphylococcus aureus* and *Staphylococcus epidermidis*. The results showed that all the compounds exhibit good inhibition potential as anti-bacterial drugs, especially compound (**3**) and compound (**4**).

1. Introduction

Recently, as is environmentally necessary, scientific attention has been directed towards greener synthesis methods with the aim of avoiding the use of toxic catalysts and solvents.[1–4] Thus, heterogeneous catalysts have been suggested as replacements for homogeneous catalysts. Heterogeneous catalysts have the advantage of being easily isolated from the reaction medium by simple filtration, enabling them to be reused. Polymeric nanocomposites have been used for base-catalyzed reactions.[5–7] Chitosan (CS) possesses excellent properties: it is biodegradable, non-toxic and insoluble in most solvents. Despite these advantages, chitosan is unable to form a film or membrane, as it forms a gel when cast.

In our previous study, aluminium oxide nanopowder was added to chitosan to increase its basicity and enhance the formation of the composite film.[7] Moreover, to increase the base characteristics of chitosan, magnesium oxide and copper oxide nanocomposites have been used as efficient catalysts for the synthesis of triazoles.[8,9]

In the present study, CS was allowed to react with diallylamine (DAA) to reduce the hydrophilicity of the polymer, thus enhancing its ability to be cast into a film. This also increases its basicity due to the presence of DAA moieties, as well as pyrrolidine rings as branches, on the CS main chains.

While CS-DAA exhibits some base characteristics, the CS-DAA–MgO nanocomposite enhances the formation of the films due to its nano size, in addition to the basicity of MgO.

Pyrazole is considered to be one of the most important heterocyclic scaffolds, as it exhibits a wide range of physiological and pharmacological properties,[10] including antibacterial,[11] anti-fungal,[12] anti-inflammatory,[13] anti-tubercular,[14] antiviral,[15]

[a] *Chemistry Department, College of Science, Imam Abdulrahman Bin Faisal University, P.O. Box 1982, 31441, Dammam, Saudi Arabia. E-mail: aabdelnaby@iau.edu.sa*
[b] *Water Treatment Unit, Basic & Applied Scientific Research Centre (BASRC), Imam Abdulrahman Bin Faisal University, P.O. Box 1982, 31441, Dammam, Saudi Arabia*

† Electronic supplementary information (ESI) available. See DOI: https://doi.org/10.1039/d2nj05513a

anti-HIV,[16] anti-tumoral,[17] anti-leishmanial,[18] anti-cancer[19] and anti-depressant[20] activities. An increase in the inhibitory characteristics of pyrazole derivatives could be accomplished through the presence of nitrogen and sulfur heteroatoms in their molecular structure, as well as through introducing benzene moieties. Furthermore, few studies have suggested pyrazole carbothioamide derivatives as corrosion inhibitors. When compared with other families of organic chemicals, pyrazoles have low toxicity and exhibit high solubility in acidic conditions, which makes them greener corrosion inhibitors. In recent decades, the synthesis of thiadiazine derivatives, as well as studies of their chemical and biological activity, have become more important, as they have been explored for their antimicrobial,[21] anti-diabetic,[22] diuretic,[23] antioxidant,[24] anti-leishmanial,[25] and antiviral[26] activities.

A synthesis of thidazines has been reported using an ultrasonic technique at 60 °C with a moderate yield.[27] Thus, our efforts have been directed towards the synthesis of a new series of thiadiazines using heterogeneous catalysts, aiming to reduce the reaction time and improve the yield percentage. Moreover, the introduction of thiadiazine to the pyrazole moiety could increase its anti-bacterial activity.[28]

Bacterial diseases can lead to death, and bacterial infections are known for their multidrug resistance properties; thus, new compounds that act as antibacterial drugs are increasingly being sought.[29] Pyrazole scaffolds have been explored as bioactive moieties. Therefore, in this study we aimed to develop novel pyrazole derivatives that would be expected to exhibit antibacterial efficiency.

The inhibition mechanisms of antibacterial drugs involve interactions with targets of specific proteins that are responsible for a specific activity such as protein synthesis or cell wall synthesis.[30,31] The interactions between the antibacterial drugs and the proteins lead to blocking of the active site of the protein, preventing the synthesis of a new protein and destroying the bacteria.[31]

Molecular docking is a very popular tool in drug discovery.[32,33] Therefore, in this work, it has been used to predict the inhibition potential of novel synthesized compounds as anti-bacteria drugs by evaluating their binding with *Escherichia coli*, *Pseudomonas aeruginosa*, *Staphylococcus aureus* and *Staphylococcus epidermidis*. Moreover, the molecular docking results help to understand the types of interactions between these compounds and the active sites of their receptors in these bacteria. The proteins used in this study are the peptide deformylase (PDF)[34–37] and transcriptional regulator (TcaR),[38] which are commonly used in designing antibacterial drugs.

In this study, a novel synthetized CS-DAA–MgO nanocomposite will be investigated as a heterogenous base catalyst and a green method to synthetize four novel pyrazole derivatives. Thus, we could predict the inhibition potentials of these compounds as antibacterial drugs.

2. Materials and methods

2.1. Materials

3-Methyl-1-phenyl-pyrazol-5-one, acetone, ethanol, ethyl bromoacetate, diallylamine, magnesium oxide (MgO) nanopowder and chitosan of medium molecular weight (85% deacetylation) were used to obtain a high percentage of NH_2 groups over the amide groups. All chemicals were purchased from Sigma Aldrich, USA. Triple-distilled water was used in the preparation of all solutions.

2.2. Instruments

2.2.1. Nuclear magnetic resonance (NMR). NMR spectra were recorded with a Bruker AVANCE III spectrometer operating at 400 MHz using DMSO-d_6.

2.2.2. Scanning electron microscopy and energy dispersive spectroscopy (SEM/EDS). The samples were analyzed using a Tescan Vega 3 scanning electron microscope with a secondary electron (SE) detector and an energy dispersive spectroscopy detector with electron backscatter diffraction (EBSD). The analysis was carried out at a voltage of 15 keV with a working distance of 10 mm between the specimen and the detector without any polishing or use of a conductive coating to determine the structure, observe the morphology and analyze the chemical composition of the sample.

2.2.3. Thermogravimetric analysis (TGA). The samples were analyzed using a simultaneous thermogravimetric and differential thermal analyzer (DTG-60H) that was programmed to operate at a heating rate of 5 °C min^{-1} between 25 °C to 500 °C under an N_2 atmosphere to determine the weight losses of the samples at high temperatures.

2.2.4. Energy-dispersive X-ray spectroscopy (EDX). An energy-dispersive X-ray fluorescence spectrometer (model EDX8000) was used to conduct elemental analysis of the samples.

2.3. Methods

2.3.1. Synthesis of the modified chitosan (CS-DAA). DAA (0.4 M) was allowed to react with 2 g of CS (medium size) in acetic acid at 60 °C in a sonicated bath (300 W) for 10 hours. The produced CS-DAA was filtered and washed thoroughly with hot methanol. The modified polymer was characterized using ^{13}C NMR (Fig. S1, ESI†).

2.3.2. Preparation of the heterogeneous catalyst (CS-DAA–MgO) nanocomposite. Subsequently, 1 g of CS-DAA was allowed to dissolve by stirring in 30 mL of 2% v/v acetic acid solution at room temperature, which afforded a 2% w/v CS-DAA solution. The pH of the resulting solution was kept between 6 and 7 by stirring in an appropriate amount of 0.1 M NaOH solution. A suspension of 0.5 g of MgO (nanopowder with <50 nm particle size, 544833 Sigma-Aldrich) in a small amount of double-distilled water was added dropwise to the polymer solution under stirring. The mixture was further stirred for 3 h at room temperature, cast into a 100 mm Teflon dish, and dried overnight at 70 °C to remove any traces of acetic acid. Finally, the obtained CS-DAA–MgO nanocomposite film was detached and then washed with distilled water.

2.3.3. Thermal studies. The thermal properties of the nanocomposite were investigated using thermogravimetry (TGA).

2.3.4. Application of the (CS-DAA–MgO) nanocomposite as a heterogeneous base catalyst. To investigate the catalytic efficiency of the nanocomposite film, in order to optimize the reaction conditions, the reaction of thiocarbazide with 3-methyl-1-phenyl-pyrazol-5-one at different weight percentages (5, 10, 20,

30 and 35%) was studied. The reaction proceeded efficiently with the assistance of ultrasonic waves (300 W).

The catalyst was added as a film (by weight) to the reactants in absolute ethanol as a solvent.

The synthesis of each of the following compounds was first attempted using the traditional method. The products took a long time (up to 6 h) to formed and had very poor yield percentages.

2.3.5. Synthesis of *N*-(3-methyl-1-phenyl-1*H*-pyrazol-5(4*H*)-ylidene)hydrazine carbothioamide (1). 3-Methyl-1-phenyl-pyrazol-5-one (0.01 mol) and thiocarbohydrazide (0.01 mol) were irradiated in EtOH with 0.05 mol of the CS-DAA–MgO catalyst for 60 min. An orange powder was obtained and recrystallized from the EtOH (yield 90%, m.p.: 125–127 °C). FT-IR (KBr, ν, cm^{-1}): 3400, 3350, 3270 (NH_2, NH), 3010, 2990 (CH), 1602 (C═N) and 1260 (C═S); ^{1}H NMR: 1.35 (s, 3H, CH_3), 2.05 (s, 2H, CH_2), 4.05 (s, 1H, NH), 4.24 (s, 2H, NH_2), 7.16 (s, 1H, NH), 7.17–8.05 (m, 5H, Ar-H). ^{13}C NMR: 12.96 (CH_3), 17.14 (CH_2), 124.42–133.19 (C-aromatic), 147.27 (C═N), 149.85 (CH_3–C═N), 180.99 (C═S) (Fig. S2 and S3, ESI†).

Anal. calcd for $C_{11}H_{13}N_6S$ (262.10): C, 50.36; H, 5.38; N, 32.04; S, 12.22%; found: C, 50.33; H, 5.40; N, 32.06; S, 12.20%.

2.3.6. Synthesis of *N*,2-bis(3-methyl-1-phenyl-1*H*-pyrazol-5(4*H*)-ylidene)hydrazine carbothioamide (2). 3-Methyl-1-phenyl-pyrazol-5-one (0.02 mol) and thiocarbohydrazide (0.01 mol) were irradiated in EtOH with 0.05 mol of the CS-DAA–MgO catalyst for 60 min. An orange powder was obtained: yield 85%, m.p.: 139–140 °C; FT-IR (KBr, ν, cm^{-1}): 3300, 3275 (2NH), 3070, 2980 (CH), 1607 (C═N) and 1282 (C═S); ^{1}H NMR: 1.60 (s, 6H, $2CH_3$), 2.45 (s, 4H, $2CH_2$), 7.32–7.85 (m, 10H, Ar-H), 7.86 (s, 2H, 2NH). ^{13}C NMR: 16.56 ($2CH_3$), 18.12 (CH_2), 25.27 ($2CH_2$), 117.86–130.15 (C-aromatic), 159.08 (2 N–C═N), 161.56 (2C═N), 188.39 (C═S) (Fig. S4 and S5, ESI†).

Anal. calcd for $C_{21}H_{22}N_8S$ (418.17): C, 60.27; H, 5.30; N, 26.77; S, 7.66%; found: C, 60.30; H, 5.28; N, 26.78; S, 7.65%.

2.3.7. Synthesis of (*E*)-5-methyl-2-(2-(3-methyl-1-phenyl-1*H*-pyrazol-5(4*H*)-ylidene)hydrazinyl)-6-(2-phenylhydrazono)-6*H*- 1,3,4-thiadiazine (3). Compound (1) (0.01 mol) and 2-oxo-*N*′-phenylacetohydrazonoyl chloride (0.01 mol) were irradiated in EtOH with 0.05 mol of the CS-DAA–MgO catalyst for 60 min. An orange powder was obtained in a yield of 92%, m.p.: 222–224 °C. FT-IR (KBr, ν, cm^{-1}): 3000, 2990 (CH), 1690 (C═O), 1590 (C═N). ^{1}H NMR: 1.69 (s, 2H, CH_2), 2.04 (s, 3H, CH_3), 3.79 (s, 3H, CH_3), 6.71–8.27 (m, 10H, Ar-H), 11.69 (s, 1H, NH). ^{13}C NMR: 12.97 (CH_3), 14.38 (CH_3), 22.92 (CH_2), 116.28–133.19 (C-aromatic), 142.52 (S–C═N), 146.41 (C═N), 153.82 (N–C═N), 159.70 (S–C═N), 164.90 (CH_2–C═N) (Fig. S6 and S7, ESI†).

Anal. calcd for $C_{20}H_{20}N_8S$ (404.15): C, 59.39; H, 4.98; N, 27.70; S, 7.93%; found: C, 59.36; H, 4.97; N, 27.73; S, 7.95%.

2.3.8. Synthesis of (*Z*)-3-((*E*)-(3-methyl-1-phenyl-1*H*-pyrazol-5(4*H*)-ylidene)amino)-2-((*E*)-(3-methyl-1-phenyl-1*H*-pyrazol-5(4*H*)-ylidene)hydrazono)thiazolidin-4-one (4). Compound (2) (0.01 mol) and ethyl bromoacetate (0.01 mol) were irradiated in EtOH with 0.05 mol of the CS-DAA–MgO catalyst) for 60 min. An orange powder was obtained (89%), m.p.: 222–224 °C. FT-IR (KBr, ν, cm^{-1}): 3000, 2990 (CH), 1690 (C═O), 1590 (C═N). ^{1}H NMR: 1.28 (s, 6H, $2CH_3$), 1.60 (s, 4H, $2CH_2$), 4.17 (s, 2H, CH_2 thiazoline), 7.37–7.80 (m, 10H, Ar-H). ^{13}C NMR: 12.28 ($2CH_3$), 22.40 (CH_2), 26.52(CH), 28.40 (S–CH_2), 116.26–133.19 (C-aromatic), 157.27 (N–C═N), 159.60 (S–C═N), 168.90 (2 N═C–CH_2), 180.99 (N–C═N), 181.26 (C═O) (Fig. S8 and S9, ESI†).

Anal. calcd for $C_{23}H_{22}N_8OS$ (458.16): C, 60.24; H, 4.84; N, 24.44; S, 6.99%; found: C, 60.25; H, 4.85; N, 24.45; S, 6.96%.

2.3.9. *In vitro* antimicrobial activity of tested compounds. Stock suspensions of tested compounds were initially prepared at a dilution of 60 mg mL^{-1} in sterile distilled water. The solutions were then homogenized by sonication for 30 min. The initial antimicrobial effect of the samples was assessed by the measurement of the inhibition zones (mm) formed in Mueller Hinton agar (MHA) according to the standard Beecher and Wong[39] method. The seeded clinical microbial strains were *Pseudomonas aeruginosa*, *Staphylococcus epidermidis*, *Escherichia coli*, and Staphylococcus aureus. The MHA was adjusted to pH 7.0 and then sterilized by autoclaving for 20 min at 121 °C. After settling the medium in Petri dishes, the selected bacteria at 1.0 × 108 CFU mL^{-1} were swabbed on the surface of an agar layer. Thereafter, filter paper disks of 5 mm in diameter were positioned onto the agar surface. The tested compounds were then applied at 5 μL per disk. Incubation of the cultures was carried out for 24 h at 37 °C. The width of the clearing zones was evaluated to verify the antimicrobial potential of the tested compounds.[40]

2.3.10. *In silico* preparation of the receptor. The structures of the target proteins of *Escherichia coli* (1BSK), *Staphylococcus aureus* (1LQW),[41] *Pseudomonas aeruginosa* (1N5N)[42] and *Staphylococcus epidermidis* (3KP3),[38] were downloaded from the Protein Data Bank (PDB) database (**https://www.rcsb.org/pdb**).[43] The water molecules, unwanted chains, co-crystallized ions and ligands were removed from the PDB files. The structures were then prepared for the docking by adding the polar hydrogen atoms and the partial charge of the system.

2.3.11. Identification of the active site. The active sites of the target proteins were recognized using Discovery Studio Visualizer software[44] and have also been obtained in previous studies.[34–38] Using Autodock tools, the docking grid box was selected to cover the active site for each receptor.

2.3.12. *In silico* preparation of the ligands. ChemSketch (ACD Labs, Toronto, ON, Canada, freeware) version 2.5[45] was used to obtain the optimized 3D structures. The structures were checked using PyMOL software version 4.2.0 (Schrodinger Inc., New York, NY, USA).[46]

2.3.13. Docking study. AutoDock-Tools (ADT) version 1.5.6 (Scripps Research, San Diego, CA, USA)[47] was used to prepare the docking PDBQT files with default settings. The Lamarckian Genetic Algorithm was utilized to perform the docking calculations for the ligands in the active sites of the receptors by using the Autodock Vina server (version 1.1.2)[48] with an exhaustiveness parameter of 32 applied to the calculations. The best binding energy for each ligand–receptor calculation was considered. Discovery Studio Visualizer software[44] was used to evaluate the type of each interaction.

3. Results and discussion

3.1. Synthesis of chitosan-diallyl amine (CS-DAA)

The synthetized (CS-DAA) was characterized using ^{13}C NMR spectroscopy, which revealed the following:

(1) A peak at 70 ppm indicated the formation of a bond between the hydroxyl group at the C6 position of chitosan and the DAA moiety.

(2) New peaks at 22, 30, and 40 ppm indicated the formation of a pyrrolidine ring through an intramolecular cyclopolymerization process[49] (Table 1).

Chitosan is unable to be cast as a film and usually forms a gel, due to its high hydrophilicity. The reaction of chitosan with DAA leads to the formation of some pyrrolidine rings through the chitosan matrix, which decreases its hydrophilicity, thus enhancing its casting into a film. Moreover, pyrrolidine rings exhibit basic characteristics due to the free lone pair of electrons belonging to the nitrogen atom, which increases the basicity of the chitosan polymeric matrix.

3.2. Fabrication of the CS-DAA–MgO nanocomposite

The XRD pattern for the nanocomposite is shown in Fig. 1. The main broad reflection at 2θ = 18–21° is characteristic of the polymer hydrated crystalline structure of modified chitosan.

Table 1 ^{13}C NMR spectral data of CS-DAA

Chitosan-diallylamine	Carbon atoms	^{13}C NMR (σ ppm)
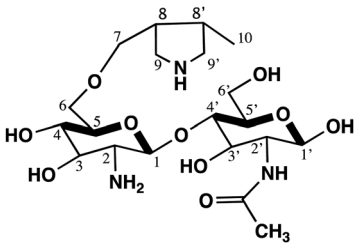	C1	104
	C2	53
	C3, C3′	73
	C4, C4′	82
	C5	78
	C6	75
	C1′	95
	C2′	59
	C5′	79
	C6′	60
	C7	70
	C8, C8′	30
	C9, C9′	40
	C10	22
	C11	173
	C12	23

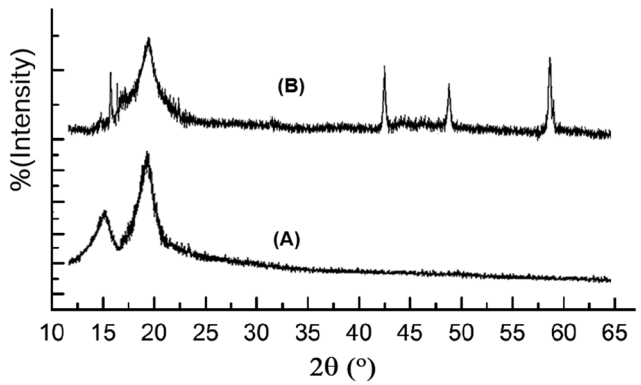

Fig. 1 XRD of CS-DAA (A) and the CS-DAA–MgO nanocomposite (B).

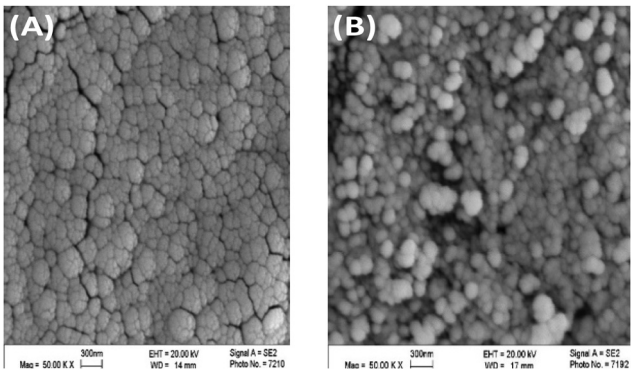

Fig. 2 SEM of CS-DAA–MgO nano composite (A) and MgO nano powder (B).

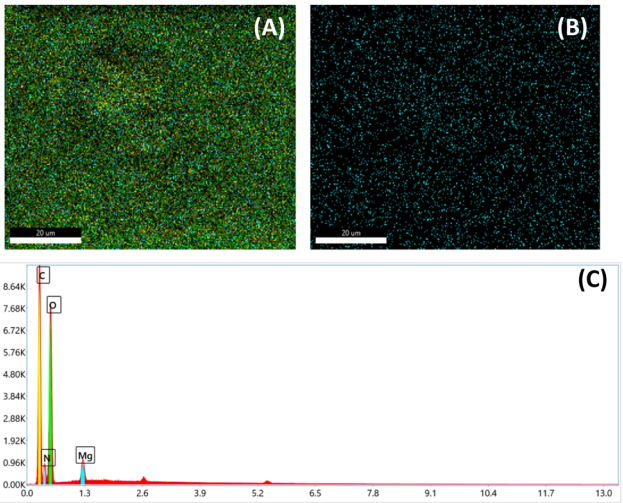

Fig. 3 EDX image of the CS-DAA–MgO (A) and nano-MgO (B), and EDX analysis of the CS-DAA–MgO nanocomposite (C).

The peaks at $2\theta \leq 15$ and the sharp peaks from 2θ = 40 to 60° are associated with MgO coordination bonds with the polymer main chains, as the MgO nanoparticles exhibit two characteristic peaks at 2θ = 43° and 60°.[50]

Fig. 2 shows the difference in the morphology of the nanocomposite (A) compared to that of MgO nanoparticles.

Fig. 3 (A) Shows the EDX image of CS-DAA–MgO, in which all the nanocomposite constituents are present, as compared to that of nano-MgO (B). The yellow color indicates carbon atoms, the pale blue nitrogen atoms, the green color oxygen atoms, and the blue color magnesium atoms. Fig. 3(A) shows the EDX image indicating the uniform distribution of the nano-MgO through the nanocomposite. The EDX analysis showing the atomic percentages in the nanocomposite is presented in Fig. 3(C).

From all the data mentioned above, a schematic representation of the CS-DAA–MgO nanocomposite could be prepared (Fig. 4).

3.3. Thermal studies

The thermal stability of the nanocomposite was investigated prior to suggesting it as a heterogenous catalyst for the synthesis

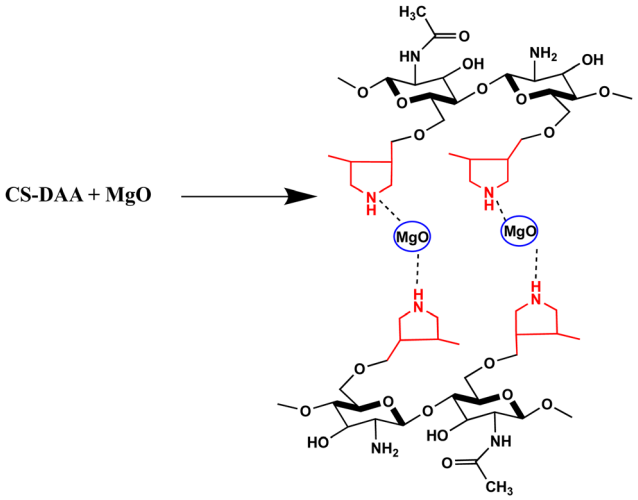

Fig. 4 Schematic representation of the CS-DAA–MgO nanocomposite.

Table 2 Comparison of the T values and weight loss percentages at high temperature of the nanocomposites with various percentages of nano-MgO as compared to CS

Polymeric material	T (°C)	Weight loss % at 500 °C
Chitosan	235	45
CS-DAA	220	36
CS-DAA–MgO (2%)	280	25
CS-DAA–MgO (5%)	295	15

of pyrazole derivatives. The results revealed that the composite exhibited higher thermal stability than the parent chitosan, as shown from the initial decomposition temperature (T), which was the temperature at which the polymer started to lose parts of its matrix, and the weight loss percentage at 500 °C. Moreover, increasing the percentage of nano-MgO powder in the nanocomposite increased its thermal stability. The 5% MgO composite exhibited a higher T value than that of the composite containing 2% (Table 2 and Fig. 5).

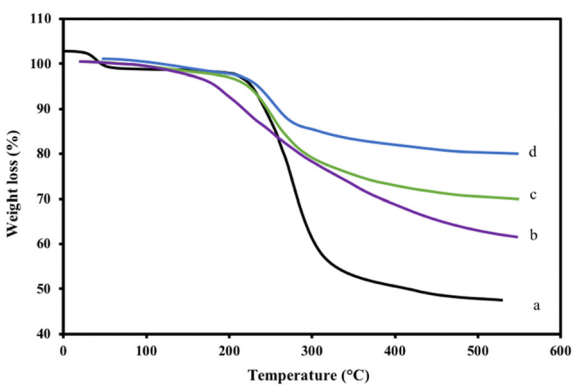

Fig. 5 TGA of the CS-DAA–MgO nanocomposites with (c) 2% nano-MgO (d) and 5% nano-MgO, along with those of (b) CS-DAA and (a) CS.

3.4. CS-DAA–MgO nanocomposite as base catalyst for the synthesis of pyrazole derivatives (1), (2), (3), and (4)

Green methods are widely used in heterocyclic chemistry. The base characteristics of the synthetized nanocomposite enable its use as a heterogeneous biodegradable catalyst for the synthesis of four pyrazole derivatives (Scheme 1).

The use of this catalyst minimized the reaction time and increased both the percentage yield and the purity of the products as compared with the traditional method. According to the literature, the removal of water is the rate-determining step.[51] Therefore, the catalyst was thought to engage in this step, as presented in Scheme 2.

The composite exhibited base characteristics because it consisted of pyrrolidine rings, the constructed branches, and the nano-sized base MgO. Thus, the composite could enhance the formation of the products in a short time with a high percentage yield. The branches of the pyrrolidine rings covered the chitosan main chains, surrounding the reactant molecules, thus enhancing their reaction.

Thus, sono-condensation of the pyrazolone derivative with thiocarbohydrazide at 70 °C in 1 : 1 and 2 : 1 ratios afforded the corresponding starting mono- and bis-thiocarbohydrazone mono- and dihydrazones (1, 2) in higher yields than the traditional methods (Scheme 1).

The structures of these hydrazones were elucidated *via* spectral data. The IR spectrum of (1) showed absorption peaks

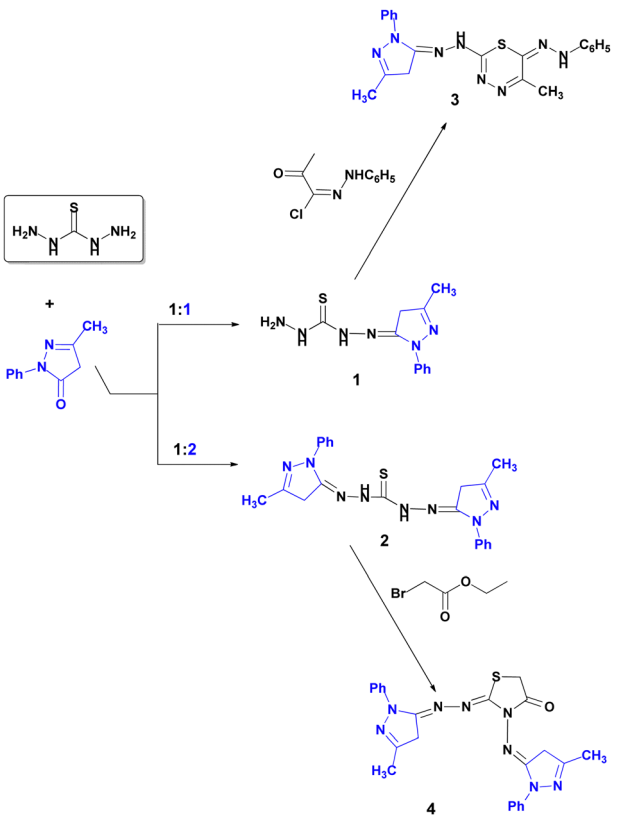

Scheme 1 Synthesis of pyrazole derivatives **1–4** using the heterogeneous base nanocomposite CS-DAA–MgO.

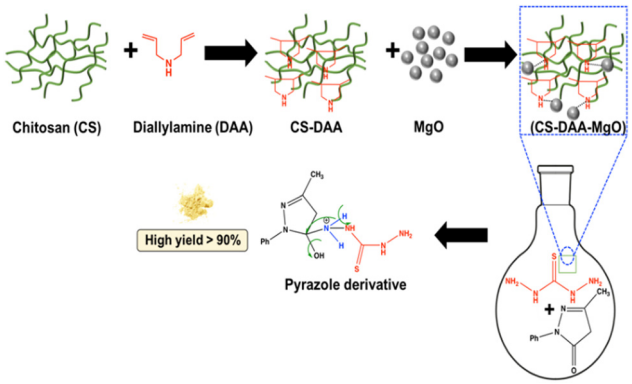

Scheme 2 Schematic representation of the role of the CS-DAA–MgO catalyst in the synthesis of compound (**1**).

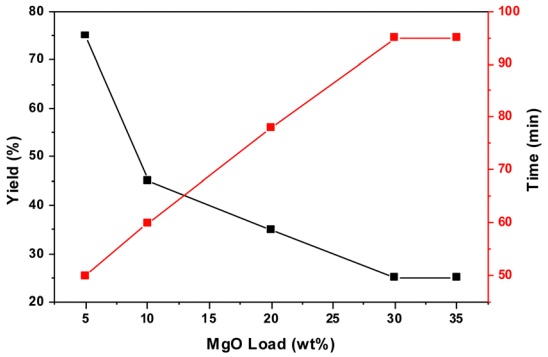

Fig. 6 Catalyst loading optimization of the CS-DAA–MgO nanocomposite catalyst.

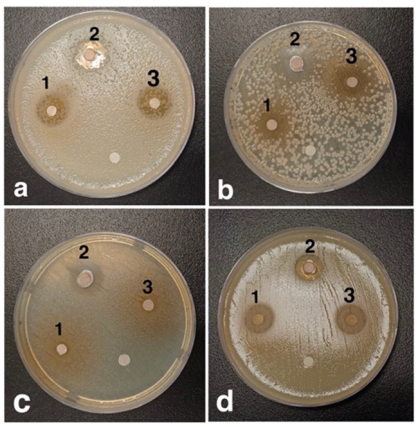

Fig. 7 Clearance zones of compounds (**1**), (**2**), and (**3**) for various bacteria: *Pseudomonas* (a), *Staphylococcus epidermidis* (b), *Escherichia coli* (c), and *Staphylococcus aureus* (d).

in the regions 3390, 3360, and 3290 cm^{-1}, which were attributed to NH_2 and the N–H functional groups. Additionally, the peak at 1260 cm^{-1} confirmed the presence of a C═S group. Furthermore, ^{1}H NMR (DMSO) of (1) showed signals at δ 4.05 and 7.16 related to the NH_2 and 2NH protons. The ^{13}C NMR spectrum (DMSO) revealed signals at 181.93 (C═S). Meanwhile, the ^{1}H NMR spectrum of dihydrazone (2) showed characteristic signals at 7.86 ppm for 2NH. The ^{13}C NMR spectrum (DMSO) exhibited signals at 188.39 (C═S).

In the present study, we achieved our targets: yields of 85% to 92% at room temperature. Moreover, the sono-reaction of (1) with hydrazonoyl halides afforded thiadiazine (3), as shown in Scheme 1. The ^{1}H NMR spectrum of (3) exhibited a signal at δ 11.69 ppm, indicating NH groups. The ^{13}C NMR spectrum (DMSO) exhibited a signal at 158.64 ppm, which confirmed the formation of a thiadiazine ring.

Finally, the cyclocondensation of bis-hydrazone (2) with ethyl bromoacetate afforded thiazolidin-4-one. The spectroscopy of compound (**4**) elucidated its structure. The IR spectrum showed a peak at 1690 cm^{-1}, which corresponds to C═O. The ^{1}H NMR spectrum of (**4**) showed a singlet signal at 4.17 (s, 2H, CH_2 thiazoline). Its ^{13}C NMR spectrum exhibited a signal at 181.93 (C═O).

3.5. Reusability of the heterogeneous of CS-DAA–MgO nanocomposite

To estimate the appropriate catalyst loading percentage, the synthesis of derivative (**2**) was tested using various catalyst loading percentages under the same reaction conditions. The results revealed that the optimum loading percentage is 30 wt% (Fig. 6).

The reusability of the catalyst was investigated by extensively washing the used catalyst with ethanol and allowing the ethanol traces to evaporate at room temperature. The results revealed that the catalyst could be reused four times without a significant loss of its catalytic activity (Fig. S10, ESI†).

3.6. Antibacterial activity

3.6.1. Antibacterial tests. Fig. 7 shows the antibacterial test for compounds **1**, **2**, and **3**. The tested compounds exerted antimicrobial activity against almost all the tested bacteria. Compound 3 appears to be the most active one.

From the lab antibacterial test, it was observed that the synthetized pyrazole derivatives exhibited high efficiencies. The following molecular docking calculations will evaluate and confirm these anti-bacterial efficiencies.

3.6.2. Molecular docking. The molecular docking study was performed to determine the inhibition potential of the four novel compounds as anti-bacterial drugs used against *Escherichia coli*, *Pseudomonas aeruginosa*, *Staphylococcus aureus and Staphylococcus epidermidis*. The results show that all the compounds have binding energy inhibition potential values between −7.0 to −9.4 kcal mol^{-1}, which are better than the binding energy inhibition potential of the reference ligand in the *Escherichia coli* active site. In addition, the binding energy inhibition potential of compounds (**2**), (**3**) and (**4**) is better than the binding energy inhibition potential of the reference ligand in *Staphylococcus epidermidis*. The binding energy of the *Escherichia coli* reference ligand is −5.6 kcal mol^{-1}, while the binding energy of the *Staphylococcus epidermidis* reference ligand is −7.3 kcal mol^{-1}. We predict that the four novel synthesized compounds can perform well as inhibitory drugs for all the bacteria proteins in this

study, especially compound (**3**) and compound (**4**). The results for each protein are presented subsequently.

3.6.2.1. Escherichia coli. The docking results of the four novel compounds were investigated and compared with the docking results of the original ligand in the active site of the protein PDB file as a reference. All four compounds present better performance than the original ligand.

Table 3 shows that compound (**1**) and compound (**2**) have binding energies of −7.2 kcal mol^{-1} and −7.7 kcal mol^{-1}, respectively.

Both compounds have several types of interactions with the residues in the active site of the receptor. Compound 1 has two hydrogen bonds with GlyA45 and GluA133, alkyl and pi–alkyl interactions with the three residues IleA44, CysA129 and IleA128, and a pi–sigma interaction with HisA132. Compound 2 has alkyl and pi–alkyl interactions with the four residues IleA91, CysA90, ArgA97 and CysA129, and one hydrogen bond with GluA42. Moreover, compound (**2**) has a pi–sigma interaction with IleA44, and a pi–pi interaction with HisA132. Compound (**3**) has the second-best binding energy for this receptor. Fig. 8 shows the interactions between the compound and the residues in the active site. It has one hydrogen bond with GluA95, and alkyl and pi–alkyl interactions with five residues: LeuA91, IleA86, IleA44, CysA129 and ProA94. In addition, there is a pi–anion interaction with GluA133 and pi–sulfur interaction with CysA90. These interactions exhibit a binding energy equal to −8.7 kcal mol^{-1}.

Fig. 9 shows the interactions between compound (**4**) and the residues in the active site. This compound has a binding energy of −9.2 kcal mol^{-1}, which is the highest affinity of all the compounds to the *Escherichia coli* active site based on the docking results.

Table 3 Binding energies of the docking between the compounds and the *Escherichia coli* receptor, the number of hydrogen bonds and the number of the residues involved in the hydrogen bonding

Compound	Binding affinity (kcal mol^{-1})	No. of H-bonds	H-bonding residues
1	−7.2	2	GlyA45, GluA133
2	−7.7	1	GluA42
3	−8.7	1	GluA95
4	−9.2	1	ArgA97

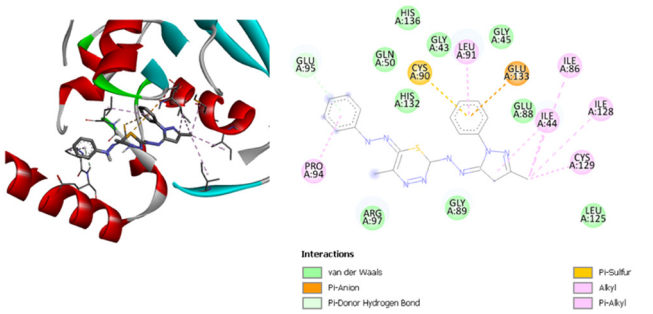

Fig. 8 3D (left) and 2D (right) images of the binding interactions of compound (**3**) with the active site of *Escherichia coli*.

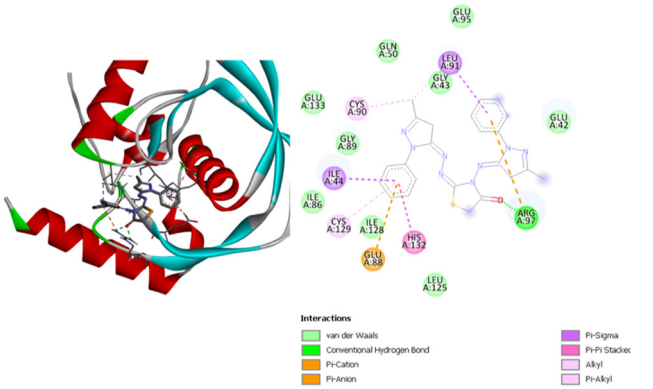

Fig. 9 3D (left) and 2D (right) images of the binding interactions of compound (**4**) with the active site of *Escherichia coli*.

Compound (**4**) has one hydrogen bond with ArgA97, as well as several other interactions including alkyl and pi–alkyl interactions with CysA90, GlyA43, and the CysA129; pi–sigma interactions with IleA44 and LeuA91; a pi–pi interaction with HisA132; and pi–cation and pi–anion interactions with GluA88 and ArgA97. All the compounds present several van der Waals interactions with different residues of the active site of the receptor. This is shown in Fig. 8 and 9 for compounds (**3**) and (**4**), respectively, and in Fig. S11 and S12 (ESI†) for compounds (**1**) and (**2**), respectively. Notably, all four compounds exerted van der Waals interactions with GlnA50 and GlyA89.

3.6.2.2. Pseudomonas aeruginosa. The docking results of the four novel compounds with the active site of the *Pseudomonas aeruginosa* protein are shown in Table 4. The most promising compounds are compound (**3**) and compound (**4**).

Compound (**1**) has the lowest binding affinity with the *Pseudomonas aeruginosa* active site, with a binding energy of −7.0 kcal mol^{-1}. This compound has two hydrogen bonds with ValA95 and CysA92. This compound also has two alkyl interactions with LeuA83 and IleA45, and one pi–pi interaction with TyrA99. On the other hand, compound (**2**) shows a better binding infinity than compound (**1**) at −7.7 kcal mol^{-1}. This compound did not show as many types of interactions as the other compounds. It has only alkyl and pi–alkyl interactions with the three residues IleA45, CysA131, and LeuA93. Fig. 10 shows the interactions between compound (**3**) and the residues in the active site. This compound has a very good binding energy. It has a binding energy of −8.0 kcal mol^{-1}. It has one hydrogen bond with TyrA99 and one pi-doner hydrogen bond

Table 4 Binding energies of the docking between the compounds and the *Pseudomonas aeruginosa* receptor, the number of hydrogen bonds and the number of the residues involved in the hydrogen bonding

Compound	Binding affinity (kcal mol^{-1})	No. of H-bonds	H-bonding residues
1	−7.0	2	ValA95, CysA92
2	−7.7	—	—
3	−8.0	2	TyrA99, TyrA88
4	−8.7	3	TyrA99, TyrA88, GlyA91

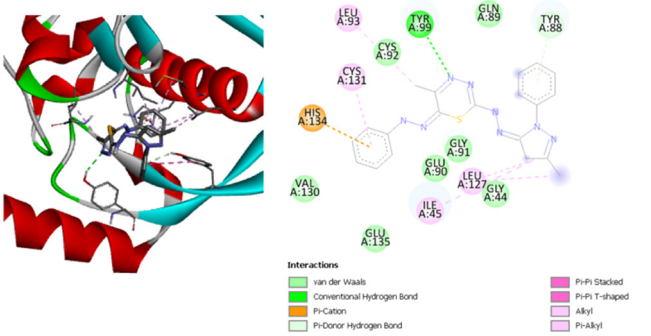

Fig. 10 3D (left) and 2D (right) images of the binding interactions of compound (**3**) with the active site of *Pseudomonas aeruginosa*.

with TyrA88. In addition, alkyl and pi–alkyl interactions with LeuA127, IleA45, LeuA93, CysA131 and a pi–cation interaction with HisA134. Compound (**4**) has the highest affinity with the *Pseudomonas aeruginosa* active site. It has a binding energy of −8.7 kcal mol^{-1}. Fig. 11 shows the interaction between the compound and the residues in the active site. It has three hydrogen bonds with TyrA99, TyrA88, and GlyA91, one pi-donor hydrogen bond with GlyA91, three pi–alkyl interactions with ProA43, TyrA99, and IleA45, and an unfavorable donor–donor interaction with IleA45. Several van der Waals interactions between these compounds have been identified from Fig. 10 and 11 for compounds (**3**) and (**4**), and from Fig. S13 and S14 (ESI†) for compounds (**1**) and (**2**). It was found that all these compounds exhibit van der Waals interactions with the two residues GluA90 and GlnA89.

3.6.2.3. Staphylococcus aureus. Table 5 shows the binding energies of the four novel compounds with the active site of *Staphylococcus aureus* protein. The most promising compounds are compound (**3**) and compound (**4**).

Compound (**1**) has a binding energy of −7.4 kcal mol^{-1}. It was found that there is one hydrogen bond with SerA57, pi–anion and pi–cation interactions with HisA154 and GluA109, and hydrophobic interactions with ValA151, LeuA112, and CysA111. Compound (2) has a binding energy equal to −7.2 kcal mol^{-1}. It has two hydrogen bonds with TypA147 and GlyA110, and alkyl and pi–alkyl interactions with the four residues LeuA105,

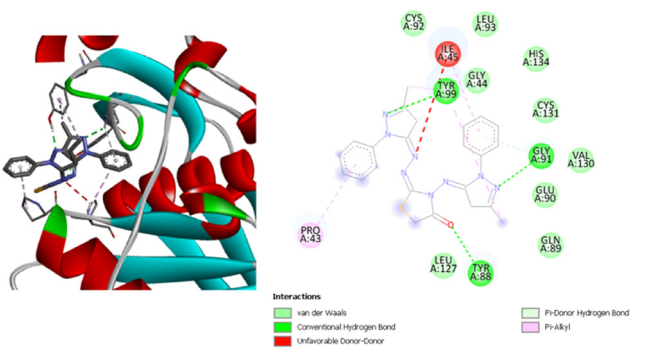

Fig. 11 3D (left) and 2D (right) images of the binding interactions of compound (**4**) with the active site of *Pseudomonas aeruginosa*.

Table 5 Binding energies of the docking between the compounds and the *Staphylococcus aureus* receptor, the number of hydrogen bonds and the number of residues involved in the hydrogen bonding

Compound	Binding affinity (kcal mol^{-1})	No. of H-bonds	H-bonding residues
1	−7.4	1	SerA57
2	−7.2	2	TypA147, GlyA110
3	−9.4	1	ValA59
4	−8.9	1	ArgA56

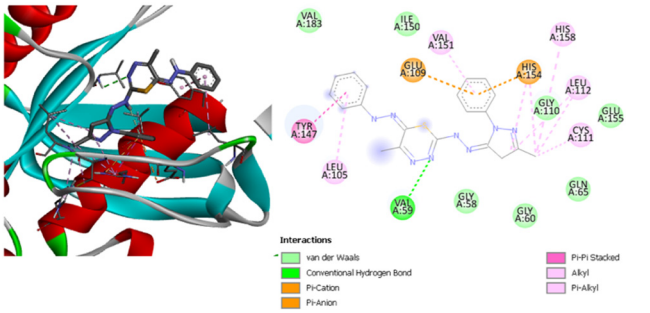

Fig. 12 3D (left) and 2D (right) images of the binding interactions of compound (**3**) with the active site of *Staphylococcus aureus*.

ValA183, ValA151 and TypA147. Fig. 12 shows the interactions between compound (**3**) and the residues in the active site of the receptor. It has a binding energy of −9.4 kcal mol^{-1}, which is the highest binding score for this protein.

It was found that there is one hydrogen bond with ValA59, two pi–cation and pi–anion interactions with GluA109 and HisA154, one pi–pi stacked interaction with TyrA147, and alkyl and pi–alkyl interactions with the four residues ValA151, HisA158, LeuA112 and CysA111. Compound (**4**) has a binding energy of −8.9 kcal mol^{-1}, which is the second highest binding score for this protein. Fig. 13 shows the interactions between this compound and the active site of the receptor. There is one hydrogen bond with ArgA56, one pi–anion interaction with GluA155, and one pi–sulfur interaction with CysA111. In addition, there is also an unfavorable donor–donor interaction with GlyA110, alkyl and pi–alkyl interactions with ValA151, HisA154, IleA150, LeuA112 and LeuA105. Fig. 12 and 13 depict the van

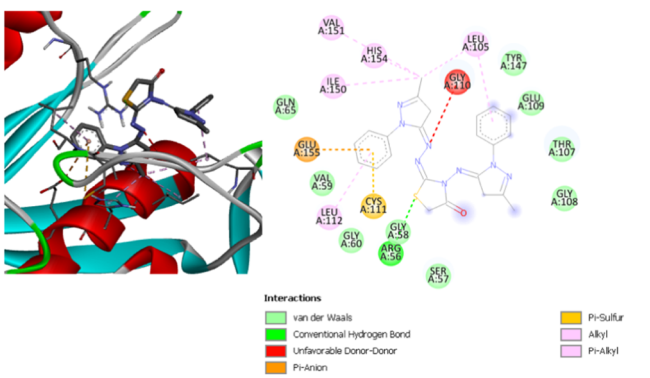

Fig. 13 3D (left) and 2D (right) images of the binding interactions of compound (**4**) with the active site of *Staphylococcus aureus*.

Table 6 Binding energies of the docking between the compounds and the *Staphylococcus epidermidis* receptor, number of the hydrogen bonds and number of the residues involved in the hydrogen bonding

Compound	Binding affinity (kcal mol^{-1})	No. of H-bonds	H-bonding residues
1	−7.0	—	—
2	−7.9	4	LysB28, GluB39, GlnA61
3	−8.9	1	HisB42
4	−9.2	3	AsnA20, AsnB20

der Waals interactions of compounds 3 and 4, while Fig. S15 and S16 (ESI†) show the van der Waals interactions of compounds **1** and **2**. It has been found that all these compounds exhibit van der Waals interactions with the residue GlyA58.

3.6.2.4. Staphylococcus epidermidis. Table 6 shows the binding energies of the four novel compounds with the active site of *Staphylococcus epidermidis* protein. The most promising compounds are compound (**3**) and compound (**4**). They perform better than the reference ligand.

Based on the docking results, compound (**1**) is shown as the least active compound with *Staphylococcus epidermidis* active site. It has a binding energy of −7.0 kcal mol^{-1}. It only has one type of interaction with the active site of the receptor. Two pi–alkyl interactions are identified with HisB42 and IleA16. On the other hand, compound (**2**) has a binding energy of −7.9 kcal mol^{-1}. It has four hydrogen bonds with LysB28, GluB39 and GlnA61, a pi–sigma interaction with AlaB38, and a pi–cation interaction with LysB28, as well as alkyl and pi–alkyl interactions with LysB25, AlaB24, and HisB42. Fig. 14 shows the interaction between compound (**3**) and the residues in the active site, with a binding energy of −8.9 kcal mol^{-1}. Compound (**3**) has one hydrogen bond with HisB42, and alkyl and pi–alkyl interactions with AlaB24, IleA16, and LeuB27. Compound (**4**) has a binding energy equal to −9.2 kcal mol^{-1}, which is the highest binding score for this protein.

Fig. 15 shows the interactions between this compound and the active site of the receptor. It was found that there are three hydrogen bonds with AsnA20 and AsnB20, one pi–sulfur interaction with HisB42, and alkyl and pi–alkyl interactions with ValA63, AlaB38, AlaB24, and HisB42. For this protein, it has been found from Fig. 14 and 15 for compounds (**3**) and (**4**), and from Fig. S17 and S18 (ESI†) for compounds (**1**) and (**2**) that all compounds have van der Waals interactions with the ThrB23 and GlnB31 residues.

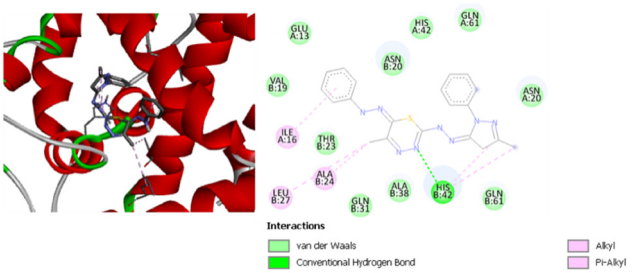

Fig. 14 3D (left) and 2D (right) image of the binding interactions of compound (**3**) with the active site of *Staphylococcus epidermidis*.

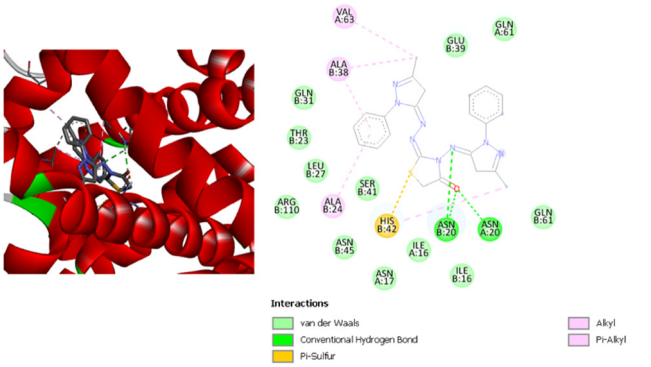

Fig. 15 3D (left) and 2D (right) image of the binding interactions of compound (**4**) with the active site of *Staphylococcus epidermidis*.

4. Conclusions

CS-DAA–MgO nanocomposite films were prepared with various percentages of nano-MgO *via* a simple solution casting method. The structure of CS-DAA was confirmed using ^{13}C NMR. The dispersed nanopowder was characterized using SEM; the whole composite film was characterized using XRD. The nanocomposite containing 5% MgO exhibited the highest thermal stability, as shown from the TGA curves. The nanocomposite (5% MgO) was used as a heterogeneous base catalyst for the green synthesis of four novel pyrazole derivatives. The optimal catalyst loading was 30%, and the catalyst was easily separated from the reaction medium after the formation of the product. The catalyst was effectively reusable up to four times without significant loss of its activity.

Under the effect of CS-DAA–MgO, pyrazolone was converted into pyrazolyl derivatives bearing hydrazones, thiadiazines, and thiazolidin-4-one moieties. The four novel pyrazole derivatives were synthetized in the minimum time and in high percentage yield. The structures of the new derivatives were elucidated *via* spectral data and elemental analysis. Moreover, their bioactivity has been explored, and they are expected to be powerful antibacterial agents, as shown from laboratory tests and confirmed by molecular docking evaluations.

The results of the molecular docking study showed that all ligands had a binding energy inhibition potential between −7.0 and −9.4 kcal mol^{-1}. The most promising compounds were compound (**3**) and compound (**4**), where the binding energy inhibition potential values were between −8.0 and −9.4 kcal mol^{-1}, which are better than the binding energy inhibition potentials of the reference ligands for *Escherichia coli* and *Staphylococcus epidermidis*. However, biological activity studies and more advanced investigations are necessary before the application of these compounds as antibacterial drugs.

Author contributions

Conceptualization, Abir S. Abdel-Naby; Sara Nabil; Sarah Aldulaijan; Salha Alharthi; data curation, Sara Nabil; Salha Alharthi; methodology, S. Abdel-Naby; Sara Nabil; Sarah Aldulaijan; Lab antibacterial test was conducted by Bushra AL Abdullatif;

formal analysis, S. Abdel-Naby; Sara Nabil; Sarah Aldulaijan; software, Sarah Aldulaijan; Salha Alharthi; writing-original draft preparation, Abir S. Abdel-Naby; Sara Nabil; Sarah Aldulaijan; supervision, Abir S. Ab-del-Naby; writing-review and editing, Abir S. Abdel-Naby; Sara Nabil; Sarah Aldulaijan; Salha Alharthi. All authors have read and agreed to the published version of the manuscript.

Conflicts of interest

There are no conflicts to declare.

Acknowledgements

The work is financially supported by institutional fund by Ministry of Education, Kingdom of Saudi Arabia, project no. IF 20-2020.

References

1 K. D. Khalil, E. I. Ibrahim and F. A. Al-Sagheer, A Novel, Efficient, and Recyclable Biocatalyst for Michael Addition Reactions and Its Iron (Iii) Complex as Promoter for Alkyl Oxidation Reactions, *Catal. Sci. Technol.*, 2016, **6**, 1410–1416.
2 K. Khalil, H. Al-Matar and M. Elnagdi, Chitosan as an Eco-Friendly Heterogeneous Catalyst for Michael Type Addition Reactions. A Simple and Efficient Route to Pyridones and Phthalazines, *Eur. J. Chem.*, 2010, **1**, 252–258.
3 K. D. Khalil and H. M. Al-Matar, Chitosan Based Heterogeneous Catalyses: Chitosan-Grafted-Poly (4-Vinylpyridne) as an Efficient Catalyst for Michael Additions and Alkylpyridazinyl Carbonitrile Oxidation, *Molecules*, 2013, **18**, 5288–5305.
4 B. Mallesham, D. Raikwar and D. Shee, The Role of Catalysis in Green Synthesis of Chemicals for Sustainable Future, *Advanced functional solid catalysts for biomass valorization*, Elsevier, 2020, pp. 1–37.
5 M. Madkour, K. D. Khalil and F. A. Al-Sagheer, Heterogeneous Hybrid Nanocomposite Based on Chitosan/Magnesia Hybrid Films: Ecofriendly and Recyclable Solid Catalysts for Organic Reactions, *Polymers*, 2021, **13**, 3583.
6 S. M. Riyadh, K. D. Khalil and A. Aljuhani, Chitosan-MgO Nanocomposite: One Pot Preparation and Its Utility as an Ecofriendly Biocatalyst in the Synthesis of Thiazoles and [1, 3, 4] Thiadiazoles, *Nanomaterials*, 2018, **8**, 928.
7 A. S. Abdel-Naby, S. Nabil, S. Aldulaijan, I. M. Ababutain, A. I. Alghamdi, S. Almubayedh and K. D. Khalil, Synthesis, Characterization of Chitosan-Aluminum Oxide Nanocomposite for Green Synthesis of Annulated Imidazopyrazol Thione Derivatives, *Polymers*, 2021, **13**, 1160.
8 P. K. Sahu, P. K. Sahu, S. K. Gupta and D. D. Agarwal, Chitosan: An Efficient, Reusable, and Biodegradable Catalyst for Green Synthesis of Heterocycles, *Ind. Eng. Chem. Res.*, 2014, **53**, 2085–2091.
9 K. D. Khalil, S. M. Riyadh, S. M. Gomha and I. Ali, Synthesis, Characterization and Application of Copper Oxide Chitosan Nanocomposite for Green Regioselective Synthesis of [1, 2, 3] Triazoles, *Int. J. Biol. Macromol.*, 2019, **130**, 928–937.
10 F. E. Bennani, L. Doudach, Y. Cherrah, Y. Ramli, K. Karrouchi and M. E. A. Faouzi, Overview of Recent Developments of Pyrazole Derivatives as an Anticancer Agent in Different Cell Line, *Bioorg. Chem.*, 2020, **97**, 103470.
11 T. Omara, B. Musau and S. Kagoya, Frugal Utilization of Flue-Cured Virginia Nicotiana Tabacum Leaf Wastes as a Vicissitudinous Substrate for Optimized Synthesis of Pyridine-3-Carboxylic Acid, *Amer. J. Hetero Chem.*, 2018, **4**, 49–54.
12 S. A. Khanum, S. Shashikanth, S. G. Sathyanarayana, S. Lokesh and S. A. Deepak, Synthesis and Antifungal Activity of 2-azetidinonyl-5-(2-benzoylphenoxy) Methyl-1, 3, 4-oxadiazoles against Seed-borne Pathogens of Eleusine Coracana (L.) Gaertn, *Pest Manag. Sci. Former. Pestic. Sci.*, 2009, **65**, 776–780.
13 M. J. N. Khadri, A. B. Begum, M. K. Sunil and S. A. Khanum, Synthesis, Docking and Biological Evaluation of Thiadiazole and Oxadiazole Derivatives as Antimicrobial and Antioxidant Agents, *Results Chem.*, 2020, **2**, 100045.
14 S. G. Kini, A. Bhat, Z. Pan and F. E. Dayan, Synthesis and Antitubercular Activity of Heterocycle Substituted Diphenyl Ether Derivatives, *J. Enzyme Inhib. Med. Chem.*, 2010, **25**, 730–736.
15 V. A. S. Pardeshi, N. S. Chundawat, S. I. Pathan, P. Sukhwal, T. P. S. Chundawat and G. P. Singh, A Review on Synthetic Approaches of Benzimidazoles, *Synth. Commun.*, 2021, **51**, 485–513.
16 M. Zhu, H. Zhou, L. Ma, B. Dong, J. Zhou, G. Zhang, M. Wang, J. Wang, S. Cen and Y. Wang, Design and Evaluation of Novel Piperidine HIV-1 Protease Inhibitors with Potency against DRV-Resistant Variants, *Eur. J. Med. Chem.*, 2021, **220**, 113450.
17 T. Legigan, E. Migianu-Griffoni, M. A. Redouane, A. Descamps, J. Deschamp, O. Gager, M. Monteil, F. Barbault and M. Lecouvey, Synthesis and Preliminary Anticancer Evaluation of New Triazole Bisphosphonate-Based Isoprenoid Biosynthesis Inhibitors, *Eur. J. Med. Chem.*, 2021, **214**, 113241.
18 M. A. S. Abdelwahid, T. Elsaman, M. S. Mohamed, S. A. Latif, M. M. Mukhtar and M. A. Mohamed, Synthesis, Characterization, and Antileishmanial Activity of Certain Quinoline-4-Carboxylic Acids, *J. Chem.*, 2019, **2019**, 1–9.
19 F. K. Keter and J. Darkwa, Perspective: The Potential of Pyrazole-Based Compounds in Medicine, *Biometals*, 2012, **25**, 9–21.
20 N. A. Abdel-Latif, Synthesis and Antidepressant Activity of Some New Coumarin Derivatives, *Sci. Pharm.*, 2005, **73**, 193–216.
21 D. S. Arora and J. Kaur, Antimicrobial Activity of Spices, *Int. J. Antimicrob. Agents*, 1999, **12**, 257–262.
22 M. C. Sabu and R. Kuttan, Anti-Diabetic Activity of Medicinal Plants and Its Relationship with Their Antioxidant Property, *J. Ethnopharmacol.*, 2002, **81**, 155–160.
23 P. Goya, J. A. Paez, I. Alkorta, E. Carrasco, M. Grau, F. Anton, S. Julia and M. Martinez-Ripoll, N-Substituted Pyrazino

[2, 3-c][1, 2, 6] Thiadiazine 2, 2-Dioxides. A New Class of Diuretics, *J. Med. Chem.*, 1992, **35**, 3977–3983.

24 N. J. Miller, J. Sampson, L. P. Candeias, P. M. Bramley and C. A. Rice-Evans, Antioxidant Activities of Carotenes and Xanthophylls, *FEBS Lett.*, 1996, **384**, 240–242.

25 C. A. Moreno-Camacho, J. R. Montoya-Torres, A. Jaegler and N. Gondran, Sustainability Metrics for Real Case Applications of the Supply Chain Network Design Problem: A Systematic Literature Review, *J. Clean. Prod.*, 2019, **231**, 600–618.

26 A. Chauhan, P. K. Sharma and N. Kaushik, Pyrazole: A Versatile Moiety, *Int. J. ChemTech Res.*, 2011, **3**, 11–17.

27 S. N. Shabaan, B. S. Baaiu, A. Abdel-Aziem and M. S. Abdel-Aziz, Ultrasound-Assisted Green Synthesis and Antimicrobial Assessment of 1, 3-Thiazoles and 1, 3, 4-Thiadiazines, *Green Chem. Lett. Rev.*, 2021, **14**, 679–688.

28 X. Zhong, X. Wang, L. Chen, X. Ruan, Q. Li, J. Zhang, Z. Chen and W. Xue, Synthesis and Biological Activity of Myricetin Derivatives Containing 1, 3, 4-Thiadiazole Scaffold, *Chem. Cent. J.*, 2017, **11**, 1–9.

29 G. J. Gabriel, A. Som, A. E. Madkour, T. Eren and G. N. Tew, Infectious Disease: Connecting Innate Immunity to Biocidal Polymers, *Mater. Sci. Eng., R*, 2007, **57**, 28–64.

30 R. B. Ghooi and S. M. Thatte, Inhibition of Cell Wall Synthesis—Is This the Mechanism of Action of Penicillins?, *Med. Hypotheses*, 1995, **44**, 127–131.

31 M. Hussain, T. Qadri, Z. Hussain, A. Saeed, P. A. Channar, S. A. Shehzadi, M. Hassan, F. A. Larik, T. Mahmood and A. Malik, Synthesis, Antibacterial Activity and Molecular Docking Study of Vanillin Derived 1, 4-Disubstituted 1, 2, 3-Triazoles as Inhibitors of Bacterial DNA Synthesis, *Heliyon*, 2019, **5**, e02812.

32 B. K. Shoichet, S. L. McGovern, B. Wei and J. J. Irwin, Lead Discovery Using Molecular Docking, *Curr. Opin. Chem. Biol.*, 2002, **6**, 439–446.

33 L. G. Ferreira, R. N. Dos Santos, G. Oliva and A. D. Andricopulo, Molecular Docking and Structure-Based Drug Design Strategies, *Molecules*, 2015, **20**, 13384–13421.

34 C. M. Apfel, H. Locher, S. Evers, B. Takács, C. Hubschwerlen, W. Pirson, M. G. P. Page and W. Keck, Peptide Deformylase as an Antibacterial Drug Target: Target Validation and Resistance Development, *Antimicrob. Agents Chemother.*, 2001, **45**, 1058–1064.

35 T. Agarwal, P. Gupta, S. Asthana and A. Khursheed, In Silico Analysis to Access the Antibacterial Effect of Thiazides on PDfs: Molecular Docking Approach, *Int. J. Pharm. Pharm. Sci.*, 2014, **6**, 387–391.

36 P. Lin, T. Hu, J. Hu, W. Yu, C. Han, J. Zhang, G. Qin, K. Yu, F. Götz and X. Shen, Characterization of Peptide Deformylase Homologues from Staphylococcus Epidermidis, *Microbiology*, 2010, **156**, 3194–3202.

37 D. J. Beecher and A. C. Wong, Identification of Hemolysin BL-Producing Bacillus Cereus Isolates by a Discontinuous Hemolytic Pattern in Blood Agar, *Appl. Environ. Microbiol.*, 1994, **60**, 1646–1651.

38 J.-C. Palomino, A. Martin, M. Camacho, H. Guerra, J. Swings and F. Portaels, Resazurin Microtiter Assay Plate: Simple and Inexpensive Method for Detection of Drug Resistance in Mycobacterium Tuberculosis, *Antimicrob. Agents Chemother.*, 2002, **46**, 2720–2722.

39 D. Mazel, S. Pochet and P. Marliere, Genetic Characterization of Polypeptide Deformylase, a Distinctive Enzyme of Eubacterial Translation, *EMBO J.*, 1994, **13**, 914–923.

40 Y.-M. Chang, W.-Y. Jeng, T.-P. Ko, Y.-J. Yeh, C. K.-M. Chen and A. H.-J. Wang, Structural Study of TcaR and Its Complexes with Multiple Antibiotics from Staphylococcus Epidermidis, *Proc. Natl. Acad. Sci. U. S. A.*, 2010, **107**, 8617–8622.

41 J.-P. Guilloteau, M. Mathieu, C. Giglione, V. Blanc, A. Dupuy, M. Chevrier, P. Gil, A. Famechon, T. Meinnel and V. Mikol, The Crystal Structures of Four Peptide Deformylases Bound to the Antibiotic Actinonin Reveal Two Distinct Types: A Platform for the Structure-Based Design of Antibacterial Agents, *J. Mol. Biol.*, 2002, **320**, 951–962.

42 A. Kreusch, G. Spraggon, C. C. Lee, H. Klock, D. McMullan, K. Ng, T. Shin, J. Vincent, I. Warner and C. Ericson, Structure Analysis of Peptide Deformylases from Streptococcus Pneumoniae, Staphylococcus Aureus, Thermotoga Maritima and Pseudomonas Aeruginosa: Snapshots of the Oxygen Sensitivity of Peptide Deformylase, *J. Mol. Biol.*, 2003, **330**, 309–321.

43 H. M. Berman, J. Westbrook, Z. Feng, G. Gilliland, T. N. Bhat, H. Weissig, I. N. Shindyalov and P. E. Bourne, The Protein Data Bank, *Nucleic Acids Res.*, 2000, **28**, 235–242.

44 BIOVIA and D. S. BIOVIA, Discovery Studio Visualizer. Available Online: **https://Discover.3ds.Com/Discovery-Studio-Visualizer-Download** (Accessed on 1 May 2021).

45 Acd/Chemsketch, ChemSketch Chemical Structure Drawing Software, Available Online: **https://Www.Acdlabs.Com/Products/Chemsketch/**(Accessed on 1 Januray 2021). Toronto, ON, Canada 2021.

46 PyMOL by Schrödinger, Available online: **https://pymol.org/2/** (accessed on 1 Januray 2021).

47 G. M. Morris, R. Huey, W. Lindstrom, M. F. Sanner, R. K. Belew, D. S. Goodsell and A. J. Olson, AutoDock4 and AutoDockTools4: Automated Docking with Selective Receptor Flexibility, *J. Comput. Chem.*, 2009, **30**, 2785–2791.

48 O. Trott and A. J. Olson, AutoDock Vina: Improving the Speed and Accuracy of Docking with a New Scoring Function, Efficient Optimization, and Multithreading, *J. Comput. Chem.*, 2010, **31**, 455–461.

49 A. A. Al-Ghamdi, S. N. Al-Harthi, A. M. EL-Sharif and A. S. Abdel-Naby, Cyclocopolymerization of N, N-Diallylammonium and N, N-Diallylguanidinium Acetate with Acrylonitrile Characterization, Thermal and Morphological Properties, *Arab. J. Sci. Eng.*, 2019, **44**, 6303–6311.

50 G. J. Safaei, S. Zahedi, M. Javid and M. A. Ghasemzadeh, MgO Nanoparticles: An Efficient, Green and Reusable Catalyst for the Onepot Syntheses of 2, 6-Dicyanoanilines and 1, 3-Diarylpropyl Malononitriles under Different Conditions, *J. Nanostruct.*, 2015, **5**, 153–160.

51 U. P. Singh, H. R. Bhat, M. K. Kumawat and R. K. Singh, Utilisation of Home Laundry Effluent (HLE) as a Catalyst for Expeditious One-Pot Aqueous Phase Synthesis of Highly Functionalised 4-Thiazolidinones, *SpringerPlus*, 2013, **2**, 1–11.